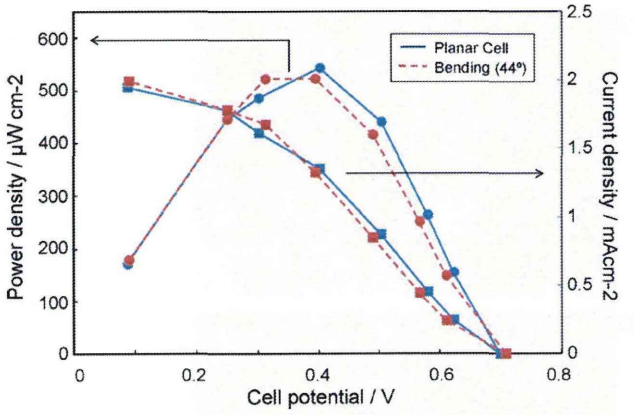

Fig. 5. Performance of the sheet-shaped biofuel cell (1 cm × 0.2 cm) with and without bending. The internal agarose layer was made with 150 mM McIlvaine buffer solution (pH 5.0) containing 200 mM fructose.

4. Conclusions

We have developed a totally flexible, sheet-shaped biofuel cell device by stacking a FDH/CNT-modified CF strip, a KB/BOD/KB-modified gas-diffusion CF strip, and an agarose hydrogel film that retains electrolyte solution and fuel (fructose). The results presented include two strategies to improve the performance of the device. (1) A CF anode modified with an appropriate CNT dispersion showed higher activity. (2) The gas-diffusion biocathode was improved by optimizing its hydrophobicity. The improved biofuel cell sheet produced a maximum power density of 550 $\mu W\,cm^{-2}$ at 0.4 V even when bent. Such a flexible, sheet-shaped power source could be combined in the future with flexible electronic to make wearable devices.

Acknowledgements

The authors thank Dr. Piotr Jasinski, Gdansk University of Technology, for his helpful advice. The carbon fabric and carbon nanotubes were kindly donated from Toho Tenax Co. and Bayer Co., respectively. This work was partly supported by the Noguchi Institute.

References

[1] I. Willner, E. Katz, Bioelectronics, Wiley-VCH, Weinheim, 2005.
[2] G.T.R. Palmore, H. Bertschy, S.H. Bergens, G.M. Whitesides, J. Electroanal. Chem. 443 (1998) 155.
[3] I. Willner, Y.M. Yan, B. Willner, R. Tel-Vered, Fuel Cell. 1 (2009) 7.
[4] M.J. Moehlenbrock, S.D. Minteer, Chem. Soc. Rev. 37 (2008) 1188.
[5] W. Gellett, M. Kesmez, J. Schumacher, N. Akers, S.D. Minteer, Electroanalysis 22 (2010) 727.
[6] A. Heller, B. Feldman, Chem. Rev. 108 (2008) 2482.
[7] S.C. Barton, J. Gallaway, P. Atanassov, Chem. Rev. 104 (2004) 4867.
[8] J.A. Cracknell, K.A. Vincent, F.A. Armstrong, Chem. Rev. 108 (2008) 2439.
[9] J. Wang, Talanta 75 (2008) 636.
[10] M.J. Cooney, V. Svoboda, C. Lau, G. Martin, S.D. Minteer, Energy Environ. Sci. 1 (2008) 320.
[11] S.A. Neto, J.C. Forti, A.R. De Andrade, Electrocatalysis 1 (2010) 87.
[12] I. Ivanov, T. Vidakovic-Koch, K. Sundmacher, Energies 3 (2010) 803.
[13] Yu E. Hao, K. Scott, Energies 3 (2010) 23.
[14] S. Rubenwolf, S. Kerzenmacher, R. Zengerle, F.V. Stetten, Appl. Microbiol. Biotechnol. 89 (2011) 1315.
[15] M.H. Osman, A.A. Shah, F.C. Walsh, Biosens. Bioelectron. 26 (2011) 3087.
[16] Y. Kamitaka, S. Tsujimura, N. Setoyama, T. Kajino, K. Kano, Physiol. Chem. Phys. 9 (2007) 1793.
[17] R.A. Bullen, T.C. Arnot, J.B. Lakeman, F.C. Walsh, Biosens. Bioelectron. 21 (2006) 2015.
[18] J. Kim, H. Jia, P. Wang, Biotechnol. Adv. 24 (2006) 296.
[19] J. Wang, Y. Lin, Trends Anal. Chem. 27 (2008) 619.
[20] E. Katz, I. Willner, Chem. Phys. Chem. 5 (2004) 1084.
[21] L. Gorton, A. Lindgren, T. Larsson, F.D. Munteanu, T. Ruzgas, I. Gazaryan, Anal. Chim. Acta 400 (1999) 91.
[22] T. Miyake, M. Oike, S. Yoshino, Y. Yatagawa, K. Haneda, M. Nishizawa, Lab Chip 10 (2010) 2574.
[23] T. Miyake, K. Haneda, N. Nagai, Y. Yatagawa, H. Onami, S. Yoshino, T. Abe, M. Nishizawa, Energy Environ. Sci. 4 (2011) 5008.
[24] F. Gao, L. Viry, M. Maugey, P. Poulin, N. Mano, Nat. Commun. 1 (2010) 2.
[25] H. Sakai, T. Nakagawa, Y. Tokita, T. Hatazawa, T. Ikeda, S. Tsujimura, K. Kano, Energy Environ. Sci. 2 (2009) 133.
[26] S. Tsujimura, A. Nishina, Y. Hamano, K. Kano, S. Shiraishi, Electrochem. Commun. 12 (2010) 446.
[27] A. Zebda, C. Gondran, A.L. Goff, M. Holzinger, P. Cinquin, S. Cosnier, Nat. Commun. 2 (2011) 370.
[28] T. Miyake, S. Yoshino, T. Yamada, K. Hata, M. Nishizawa, J. Am. Chem. Soc. 133 (2011) 5129.
[29] H. Nishide, K. Oyaizu, Science 319 (2008) 737.
[30] J.A. Rogers, T. Someya, Y. Huang, Science 327 (2010) 1603.
[31] M. Tominaga, C. Shirakihara, I. Taniguchi, J. Electroanal. Chem. 610 (2007) 1.
[32] S. Shleev, J. Tkac, A. Christenson, T. Ruzgas, A.I. Yaropolov, J.M. Whittaker, L. Gorton, Biosens. Bioelectron. 20 (2005) 2517.

Electrochemistry
The Electrochemical Society of Japan
Received: November 16, 2011
Accepted: February 4, 2012
Published: May 5, 2012
http://dx.doi.org/10.5796/electrochemistry.80.318
JOI:JST.JSTAGE/electrochemistry/80.318
Communication
Electrochemistry, **80(5)**, 318–320 (2012)

An Oxygen Responsive Microparticle-Patterned Hydrogel Sheet for Enzyme Activity Imaging

Kuniaki NAGAMINE,[a,b] Shuntaro ITO,[a] Mai TAKEDA,[a] Shingo OTANI,[a] and Matsuhiko NISHIZAWA[a,b,*]

[a] *Department of Bioengineering and Robotics, Graduate School of Engineering, Tohoku University, 6-6-01 Aramaki, Aoba-ku, Sendai 980-8579, Japan*
[b] *JST-CREST, Sanbancho, Chiyoda-ku, Tokyo 102-0075, Japan*

* *Corresponding author: nishizawa@biomems.mech.tohoku.ac.jp*

ABSTRACT

A patch-type oxygen imaging sheet useful for in vitro cellular metabolic assays was developed. Oxygen-responsive fluorescent microbeads were embedded into a biocompatible polyacrylamide gel sheet, which can be directly attached onto target cells for fluorescent imaging of metabolic activity. The sensor beads were directed in a microfluidic device using AC and DC electric manipulation techniques, followed by encapsulation in a hydrogel. Fluorescent imaging of oxygen-consuming activity was demonstrated for glucose oxidase-modified microparticles as cellular models to show the applicability of the imaging sheet to bioassays.

Keywords : Electrohydrodynamics, Microfluidic Device, Oxygen Imaging Sheet

1. Introduction

In vitro bioassays of cellular metabolic activity have been carried out to investigate the cell physiology. Evaluation of the oxygen-consuming activity of cells is significant for the indirect investigation of glucose metabolic activity. Such oxygen sensing would be applicable for revealing the mechanism of controlling blood glucose homeostasis and pathogenesis of type 2 diabetes using an insulin-responsive skeletal muscle cell.

In recent years, 2D fluorescent imaging sheets have been actively developed for mapping metabolite distribution in tissues.[1–4] In particular, Wolfbeis et al.[2,3] showed the applicability of pH- and oxygen-responsive sheets in animal experiments. All previous work used sheets in which the sensor microparticles were uniformly dispersed. However, the metabolite diffusion area is confined to the immediate vicinity of the cells. Besides, uniformly dispersed particles modify the characteristics of the hydrogel such as flexibility and nutrient permeability,[5] which will affect muscle cellular contractility and metabolic activity. In this study, the sensor beads were localized on the surface of the imaging sheet using AC and DC electric manipulation techniques to increase the surface sensitivity without sacrificing the merits of original gel characteristics. Fluorescent imaging of oxygen-consuming activity was demonstrated for glucose oxidase (GOD)-modified particles as cellular models (Fig. 1). When GOD-catalyzed glucose oxidation consumes the oxygen, the fluorescent intensity of the sensor beads increases in a pattern representing GOD activity.

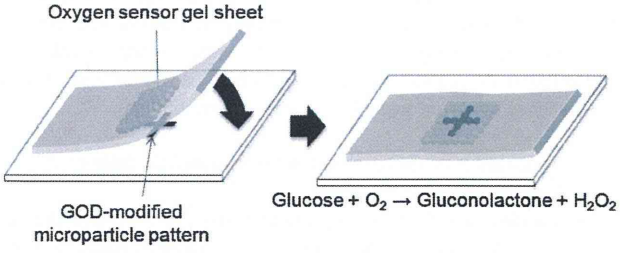

Figure 1. Schematic view of oxygen imaging around the pre-patterned GOD-modified microparticles.

2. Experimental

2.1 Preparation of oxygen responsive microparticles

A 3.5 mL of aqueous polystyrene microparticle suspension (1.0 μm diameter, Micromod) was mixed with 1.5 mL of tetrahydrofuran (THF) under ultrasonication for 10 min to swell the particles. A 0.5 mL solution of oxygen responsive fluorescent dye, platinum octaethylporphyrin (PtOEP, Sigma-Aldrich), dissolved in dimethyl sulfoxide was added to the particle suspension followed by another 20 min ultrasonication to incorporate the PtOEP into the particles.[6] Then, THF in the mixture was evaporated for 12 h at room temperature. The particles were separated by centrifugation, and washed two times with ethanol.

2.2 Fabrication of the microfluidic device

The microfluidic device was composed of three layers; an ITO top layer, a silicone rubber middle layer, and an ITO bottom layer covered with a negative photoresist SU-8 3005 pattern as an insulator. The silicone rubber layer had a stenciled opening that became the interior of the microchannel when sandwiched between the top and bottom ITO layers. The resulting microchannel was 10 mm in width and 500 μm in height. The channel inlet was connected to the particle suspension reservoir, and its outlet was attached to a syringe pump (World Precision Instruments) to introduce the particles into the channel.

2.3 Fabrication of the oxygen imaging sheet

The oxygen-responsive microparticles suspended in 0.5 mM NaCl solution were injected into the microchannel, and a sinusoidal AC voltage (100 Hz, 10 Vpp) was applied between the top and bottom ITO electrodes (Fig. 2A). The resulting AC electric field is strongest on the surface of the bottom ITO electrode, and the electrohydrodynamic force induces particle motion toward the bottom ITO pattern (1 mm × 1 mm). Then, the power supply was

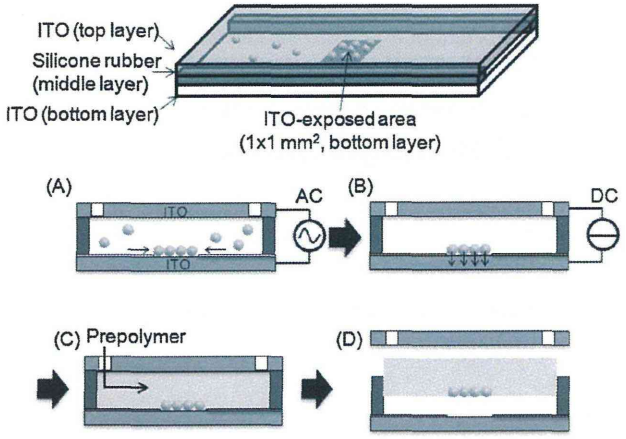

Figure 2. Preparation of the hydrogel sheet with patterned oxygen-responsive microparticles.

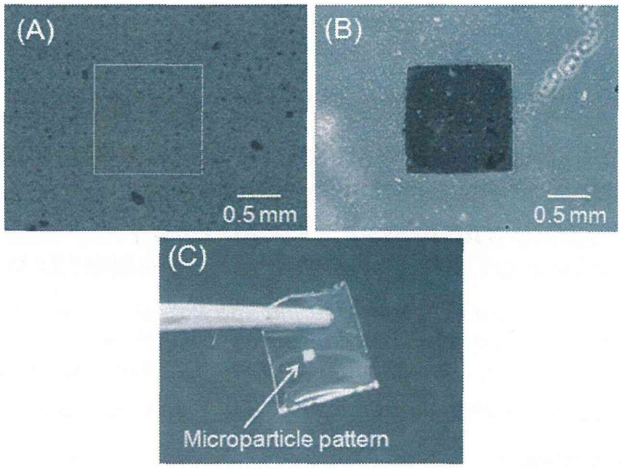

Figure 3. (A, B) Phase contrast micrographs (A) before and (B) after application of AC voltage between the top and bottom ITO electrodes. White-dashed line in (A) represents the ITO pattern on the bottom of the microchannel. (C) Photograph of the polyacrylamide hydrogel sheet with the oxygen responsive microparticle pattern embedded.

switched to 2.0 V DC to fix the patterned particles on the bottom ITO surface (Fig. 2B). After flushing out any unattached particles, the 20% (w/v) acrylamide and 1% (w/v) bis-acrylamide monomers including 0.4 vol% ammonium persulfate and 0.1 vol% tetramethylethylenediamine were injected into the channel. The device was left undisturbed for 2 h at room temperature to facilitate gelation (Fig. 2C).[7] The resulting sheet was cut into square (10 mm × 10 mm). The fluorescence of the particles was monitored using a fluorescent microscope (Olympus). The particles were excited at 520–550 nm using a mercury lamp and a bandpass filter, and a broad fluorescence emission was observed at around 650 nm.

2.4 Preparation of GOD-modified microparticle pattern on a glass substrate

Amino-functionalized microparticle suspension (1.0 μm diameter, Micromod) was dropped onto the stencil-attached aminosilanized glass substrate and evaporated overnight. The stencil sheet (100 μm thick) has a cross-formed line pattern (line width: 300 μm) made by a cutting plotter (Graphtech). An 8% glutaraldehyde solution was poured onto the particles for 1 h at room temperature to covalently immobilize the particles on the substrate and to functionalize the residual amines on the particles with glutaraldehyde. After washing away the unreacted glutaraldehyde, 1 mg/mL GOD (Wako Pure Chemicals Co.) suspended in PBS(−) (pH 7.0) was poured onto the particles and reacted at 4°C overnight to covalently immobilize the GOD onto the particles. By peeling off the stencil, the GOD-modified microparticle pattern was left on the substrate. 50 mM D-glucose dissolved in PBS(−) was dropped onto the GOD pattern to previously initiate the glucose oxidation. Then, the oxygen imaging sheet was put on the GOD pattern to obtain fluorescent image of oxygen-consuming activity.

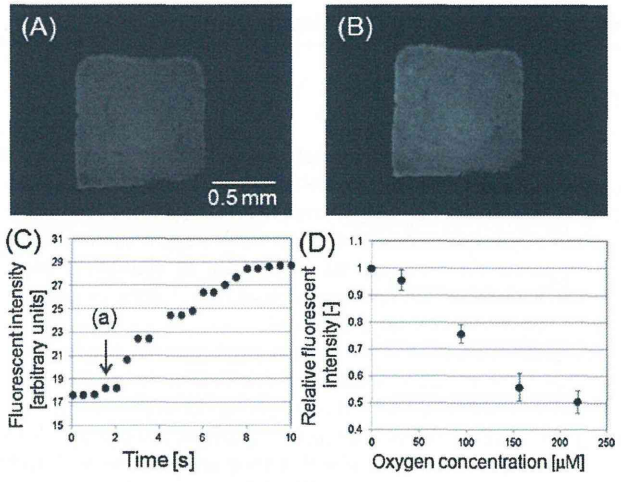

Figure 4. (A, B) Fluorescent images of the oxygen responsive microparticles in PBS(−) at a dissolved oxygen concentration of (A) 185 μM and (B) 0 μM. (C) Typical time-course of the fluorescent intensity change when Na_2SO_3 solution was added into PBS(−) at point (a). (D) Relationship between the relative fluorescent intensity of the imaging sheet and the dissolved oxygen concentration. Oxygen concentration was controlled by gradually adding Na_2SO_3 solution into the previously air-bubbled PBS(−). Each point represents the mean of three measures ± SD.

3. Results and Discussion

Figure 3 shows snapshots over time of the microparticle patterning using electrohydrodynamic force. Microparticles were introduced into the microchannel to be monodispersed (Fig. 3A). Upon application of the AC electric field, the particles rapidly moved toward the exposed ITO rectangular pattern (Fig. 3B). As demonstrated by several researchers, the application of a low frequency AC electric field drives the particles to move in a direction transverse to the field (toward the bottom ITO electrode pattern) via electrohydrodynamic fluid flow, and the particles accumulate in a two-dimensional ordered structure near the electrode surface.[8] Then, the power supply was switched to DC voltage to immobilize the negatively-charged polystyrene particles on the electrode during the solution change from water to a polyacrylamide prepolymer. Figure 3C shows a photograph of the polyacrylamide hydrogel sheet embedded with the rectangular-shaped sensor particle pattern. The particle transfer efficiency from the ITO electrode surface to the hydrogel was almost 100%.

Figure 4A shows fluorescent images of the oxygen-responsive particles on the hydrogel immersed in PBS(−) dissolving 185 μM oxygen. Oxygen-responsive dye, PtOEP, encapsulated into the particles is based on the ability of molecular oxygen to quench the dye selectively.[9] Therefore, the fluorescent intensity increases as the oxygen concentration decreases. As expected, when Na_2SO_3

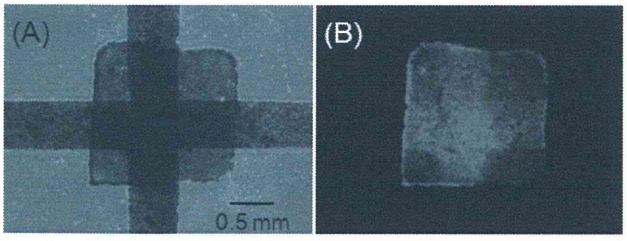

Figure 5. Phase-contrast (A) and fluorescent micrographs (B) of the oxygen imaging sheet attached to the cross-formed GOD-modified microparticles.

(an oxygen scavenger) was added, fluorescent intensity increased (Fig. 4B). 100% response was observed in 6.3 ± 1.2 s after addition of Na_2SO_3 (n = 3, Fig. 4C). Figure 4D shows the inverse relationship between the relative fluorescent intensity of the imaging sheet and the dissolved oxygen concentration measured with a DO meter (Horiba Ltd.). The relative fluorescent intensity indicates the ratio between the fluorescent intensity detected in the absence and the presence of each concentration of oxygen. This result indicated that the gel-sheet can serve as an imaging sensor for dissolved oxygen. The stability of the sensor response was evaluated by measuring the relative fluorescent intensity for PBS(−) every day for a week, showing only 4.2% decrease after 1 week.

Figure 5 demonstrates fluorescent imaging of a GOD-modified microparticle pattern using the oxygen imaging sheet. The imaging sheet was directly attached onto the GOD pattern (Fig. 5A). As can be seen in Fig. 5B, the cross-formed fluorescence displayed corresponds to the GOD pattern. We confirmed there was no response of the imaging sheet against pH change which will be induced by H_2O_2 generation during GOD-catalyzed glucose oxidation. These results suggested that GOD activity was successfully imaged using this patch-type imaging sheet. Non-uniform cross image would be attributed to non-uniform distribution of GOD beads or oxygen sensor beads. Now we are carrying out to optimize electric manipulation of the beads to obtain uniform images.

As mentioned in Introduction, oxygen sensing can be applicable to the study of type 2 diabetes using skeletal muscle cells. Our previous study of scanning electrochemical microscope (SECM) imaging using HeLa cell, which has similar basal respiratory activity with skeletal muscle myoblast,[10] has shown that the difference between the oxygen concentration at the cell surface and the bulk solution far from the cell was ~40 μM.[11] This value corresponds to 0.03 of detectable change in relative fluorescent intensity from the value at bulk oxygen concentration (~200 μM) as estimated from Fig. 4D. The muscle cells enhance their respiratory activities depending on their contractile activities, promising to obtain clear image of contraction-dependent respiratory activity of the cells. During cellular contraction, the sensor beads on the flexible imaging sheet would contract synchronously with the motion of the cells.[12] This characteristic enables continuous monitoring of respiratory activity at same position on the cell surface without concern for disturbance of oxygen concentration gradient around the contracting cells that can cause adverse effect on several oxygen imaging techniques such as SECM.

4. Conclusion

In this study, a patch type oxygen imaging hydrogel sheet was developed. For effective detection of the metabolites in the vicinity of target cells sustaining original hydrogel characteristics, the oxygen sensor beads were locally patterned on the surface of the hydrogel using the electric manipulation technique. We successfully imaged oxygen-consumption activity of GOD pattern as a cellular model, suggesting applicability of the imaging sheet to metabolic bioassays. This flexible sensor sheet is useful for glucose metabolic activity imaging of contracting skeletal muscle cells with supporting cellular contraction to study the relationship between exercise and metabolic activity of muscle in type 2 diabetes.[13]

Acknowledgment

This work was supported by a Core research for Evolutional Science and Technology grant from the Japan Science and Technology Agency.

References

1. M. I. J. Stich, L. H. Fischer, and O. S. Wolfbeis, *Chem. Soc. Rev.*, **39**, 3102 (2010).
2. S. Schreml, R. J. Meier, O. S. Wolfbeis, T. Maisch, R. M. Szeimies, M. Landthaler, J. Regensburger, F. Santarelli, I. Klimant, and P. Babilas, *Exper. Dermat.*, **20**, 550 (2011).
3. S. Schreml, R. J. Meier, O. S. Wolfbeis, M. Landthaler, R. M. Szeimies, and P. Babilas, *Proc. Natl. Acad. Sci. USA*, **108**, 2432 (2011).
4. S. Kimura, K. Matsumoto, K. Mineura, and T. Itoh, *J. Neurol. Sci.*, **258**, 60 (2007).
5. W. Lee, N. J. Cho, A. M. Xiong, J. S. Glenn, and C. W. Frank, *Proc. Natl. Acad. Sci. USA*, **107**, 20709 (2010).
6. X. D. Wang, H. H. Gorris, J. A. Stolwijk, R. J. Meier, D. B. M. Groegel, J. Wegener, and O. S. Wolfbeis, *Chem. Sci.*, **2**, 901 (2011).
7. M. Suzuki, T. Yasukawa, H. Shiku, and T. Matsue, *Langmuir*, **23**, 4088 (2007).
8. K. H. Bhatt, S. Grego, and O. D. Velev, *Langmuir*, **21**, 6603 (2005).
9. K. Montage, K. Komori, F. Yang, T. Tatsuma, T. Fujii, and Y. Sakai, *Photochem. Photobiol. Sci.*, **8**, 1529 (2009).
10. T. C. O'Riordan, A. V. Zhdanov, G. V. Ponomarev, and D. B. Papkovsky, *Anal. Chem.*, **79**, 9414 (2007).
11. M. Nishizawa, K. Takoh, and T. Matsue, *Langmuir*, **18**, 3645 (2002).
12. S. Sekine, Y. Ido, T. Miyake, K. Nagamine, and M. Nishizawa, *J. Am. Chem. Soc.*, **132**, 13174 (2011).
13. K. Nagamine, T. Kawashima, S. Sekine, Y. Ido, M. Kanzaki, and M. Nishizawa, *Lab Chip*, **11**, 513 (2011).

平成25年度

Acta Biomaterialia 10 (2014) 680–687

Contents lists available at ScienceDirect

Acta Biomaterialia

journal homepage: www.elsevier.com/locate/actabiomat

A polymeric device for controlled transscleral multi-drug delivery to the posterior segment of the eye

Nobuhiro Nagai [a], Hirokazu Kaji [b], Hideyuki Onami [a,c], Yumi Ishikawa [a], Matsuhiko Nishizawa [b], Noriko Osumi [d], Toru Nakazawa [c], Toshiaki Abe [a,*]

[a] Division of Clinical Cell Therapy, United Centers for Advanced Research and Translational Medicine (ART), Tohoku University Graduate School of Medicine, 2-1 Seiryo-machi, Aoba-ku, Sendai 980-8575, Japan
[b] Department of Bioengineering and Robotics, Graduate School of Engineering, Tohoku University, 6-6-01 Aramaki, Aoba-ku, Sendai 980-8579, Japan
[c] Department of Ophthalmology, Tohoku University Graduate School of Medicine, 1-1 Seiryo-machi, Aoba-ku, Sendai 980-8574, Japan
[d] Division of Developmental Neuroscience, United Centers for Advanced Research and Translational Medicine (ART), Tohoku University Graduate School of Medicine, 2-1 Seiryo-machi, Aoba-ku, Sendai 980-8575, Japan

ARTICLE INFO

Article history:
Received 28 August 2013
Received in revised form 26 October 2013
Accepted 8 November 2013
Available online 15 November 2013

Keywords:
Transscleral delivery
Multi-drug delivery
Retina
Poly(ethyleneglycol) dimethacrylate

ABSTRACT

The design of drug delivery systems that can deliver multiple drugs to the posterior segment of the eye is a challenging task in retinal disease treatments. We report a polymeric device for multi-drug transscleral delivery at independently controlled release rates. The device comprises a microfabricated reservoir, controlled-release cover and three different fluorescent formulations, which were made of photopolymeized tri(ethyleneglycol)dimethacrylate (TEGDM) and poly(ethyleneglycol)dimethacrylate (PEGDM). The release rate of each fluorescent is controlled by varying the PEGDM/TEGDM ratio in its formulation and the cover. The release kinetics appeared to be related to the swelling ratio of the PEGDM/TEGDM polymers. When the devices were implanted onto rat sclerae, fluorescence was observable in the ocular tissues during 4 weeks' implantation and distributed locally around the implantation site. Our polymeric system, which can administer multiple compounds with distinct kinetics, provides prolonged action and less invasive transscleral administration, and is expected to provide new tools for the treatment of posterior eye diseases with new therapeutic modalities.

1. Introduction

Diseases of the posterior eye segments cause impaired vision and blindness for millions of patients around the world [1]. There has been an increase in the understanding of the disease processes, and multiple factors have been reported to play a role in the diseases [2–4]. Thus, multi-drug therapy has become the primary method of disease management, because it offers the major advantages of enhanced efficacy of treatment, reduction of each drug dose, and mitigation of toxicity and side-effects caused by high doses of single drugs [5–7]. Multiple drugs have been used to treat patients with glaucoma [5,6] and to suppress choroidal neovascularization in patients with age-related macular degeneration (AMD) [7]. The regulation of neovascularization has received much attention, and it is now known that its balance is maintained by more than two dozen cytokines [8]. Thus it would be more effective and reasonable to use a number of drugs to treat such disease processes. Some techniques and novel pharmacological agents offer promise for the future treatment of posterior eye segment diseases [9–11]. However, the successful treatment of some retinal diseases has been limited. The limitation may be partially related to inadequate drug delivery systems for the retina, including multiple drug administration.

The principal route for local ophthalmic drug delivery remains topical application [12]. However, drug delivery to intraocular tissue by this approach is limited by the significant barrier of corneal epithelium and tear fluid turnover [13]. Systemic drug administration is not a viable alternative due to the blood–retinal barrier that limits drug access to the posterior tissues of the eye. Although intravitreal injections and intraocular implants may deliver drugs effectively to the retina and choroid, this approach is invasive to the eye and may cause severe adverse effects, such as endophthalmitis and retinal detachment [14]. Periocular or transscleral routes are less invasive than intravitreal administration and provide higher retinal and vitreal drug bioavailability (~0.01–0.1%) compared to eye drops (about 0.001% or less) [15,16]. Due to the high degree of hydration and low cell density of the sclera, soluble substrates readily pass through the sclera, although the ease of penetration of the drug to the vitreous cavity is dependent on the thickness

* Corresponding author. Tel./fax: +81 22 717 8234.
E-mail address: toshi@oph.med.tohoku.ac.jp (T. Abe).

1742-7061/$ - see front matter © 2013 Acta Materialia Inc. Published by Elsevier Ltd. All rights reserved.
http://dx.doi.org/10.1016/j.actbio.2013.11.004

of the sclera [17]. Thus transscleral delivery has the potential to be a more effective and less invasive route for intraocular drug delivery.

Several potential carriers for ocular drug delivery such as micelles [18], microneedles [19], nano- or microparticles [20,21], liposomes [22,23] and hydrogel systems [24,25] have been investigated. All the systems are injectable for localized and targeted delivery of drugs to the desired site and biodegradable to avoid a second procedure for implant removal. However, release profiles for biodegradable systems are generally complex with burst effects, i.e. an initial burst, a diffusional release phase and a final burst [26]. Additionally, the release period of such biodegradable systems is limited to less than 2 weeks [25]. In chronic eye diseases such as AMD and retinitis pigmentosa, duration of effect with controlled drug release is critical. Although several systems for multi-drug delivery have been developed [27–32], there are none intended for ocular multi-drug delivery.

In this work, we manufactured a polymeric device for multi-drug transscleral delivery to the posterior segment of the eye at independently controlled release rates (Fig. 1). The device comprises a microfabricated reservoir, controlled-release cover and drug formulations, which were made of photopolymeized tri(ethyleneglycol)dimethacrylate (TEGDM) and poly(ethyleneglycol)dimethacrylate (PEGDM). Here, we show that the release of multiple drugs can be tuned by changing the formulations of the drug as well as the covering, and demonstrate the transport of drugs into the ocular tissue in rats using fluorescents.

2. Materials and methods

2.1. Materials

PEGDM (*Mn* 750), TEGDM (*Mw* 286.3) and 2-hydroxy-2-methylpropiophenone were purchased from Aldrich (USA). Polydimethylsiloxane (PDMS), fluorescein (FL, *Mw* 332.31), rhodamine-B (Rho, *Mw* 479.02) and 4,6-diamidino-2-phenylindole dihydrochloride (DAPI, *Mw* 350.25) were purchased from Wako (Japan).

2.2. Device fabrication

The device consists of a reservoir that can contain different types of sustained release formulations and is sealed with a controlled release cover (Fig. 1c). PEGDM and TEGDM including 1% 2-hydroxy-2-methylpropiophenone as a photoinitiator were used for device materials. For the preparation of the reservoir, TEGDM prepolymer was poured into the PDMS mold fabricated via a microfabrication technique using a microprocessing machine (MicroMC-2, PMT Co.) (Supplementary Fig. S.1), and photopolymerized for 3 min with UV light (HLR400F-22, Sen Lights) at an intensity of 7.4 mW cm^{-2}. After loading the drugs, a reservoir cover was prepared by applying a prepolymer mixture of the required concentrations of PEGDM and TEGDM to the reservoir, followed by UV curing for 3 min. For the preparation of the fluorescent formulations, the fluorescents were combined with a mixture of a predetermined ratio of PEGDM and TEGDM and poured into PDMS molds and photopolymerized for 3 min. All fluorescent formulations had a fluorescent concentration of 50 mg ml^{-1} and the volume was 1.2 μl (60 μg) or 0.4 μl (20 μg) for single-fluorescent delivery or multi-fluorescent delivery devices, respectively. The dimensions of the device were 2 mm × 2 mm × 1 mm (external) and 1.55 mm × 1.55 mm × 0.5 mm (internal; maximum loading volume, 1.2 μl). PEGDM/TEGDM prepolymer mixture ratios of 100%/0%, 80%/20%, 60%/40%, 40%/60%, 20%/80% and 0%/100% were designated as P100, P80, P60, P40, P20 and P0, respectively.

2.3. Characterization of diffusion mechanism through the PEGDM/TEGDM system

The permeability of FL in phosphate-buffered saline (PBS) (0.5 mg ml^{-1}, 20 μl) through the PEGDM/TEGDM reservoir (4 mm × 4 mm × 1.5 mm, internal) was assessed by monitoring the increase in fluorescence in the external PBS (1 ml) solution with time ($n = 5$). To characterize the diffusion mechanism through the PEGDM/TEGDM system, we determined the swelling ability of the PEGDM/TEGDM polymers. The samples (size: 5 mm × 5 mm × 2 mm) with various PEGDM/TEGDM ratios were weighed in air before (W_b) and after (W_a) immersion for 24 h in 10 ml of PBS, and the swelling ratio ($W_a/W_b \times 100$) was calculated ($n = 5$).

2.4. In vitro release study

For the single delivery study, FL was pelletized with P60 and loaded in the device, followed by sealing with P100, P60 or P40 covers. For the multiple delivery, three types of fluorescents, FL, Rho and DAPI, were pelletized each with different ratios of PEGDM/TEGDM and loaded in the device, followed by sealing with P100 or P60 covers. The devices were each incubated in 1 ml of PBS at 37 °C. To estimate the amounts of fluorescent that had diffused out of the devices, the fluorescence intensities of the PBS solutions

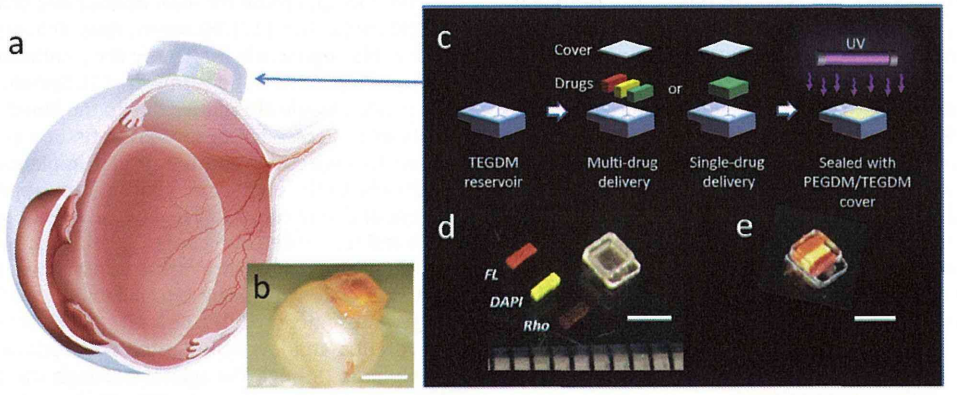

Fig. 1. (a) Schematic image of transscleral intraocular multi-drug delivery using a polymeric device placed on the sclera. (b) Photograph of the rat eye where the device was implanted on the sclera for 3 days. (c) Image shows assembling process of the device that consists of three kinds of fluorescents pelletized with PEGDM/TEGDM, a reservoir made of TEGDM and a controlled release cover made of PEGDM/TEGDM. After loading the pellets in the reservoir, the cover was sealed on the reservoir by UV curing. (d) Photographs showing three kinds of fluorescent pellets, including FL, Rho and DAPI, and a reservoir before assembling, and (e) the device after assembling. Scale bars, 2 mm.

were measured spectrofluorometrically (FluoroscanAscent; Thermo), where fluorescence excitation (ex) and emission (em) for FL, Rho and DAPI was measured at ex. 485 nm/em. 538 nm, ex. 544 nm/em. 590 nm and ex. 355 nm/em. 460 nm, respectively ($n = 6$). The PBS was replenished during the course of the release study to ensure that the concentration of fluorescent molecules was below 20% of its saturation value at all times. The results were expressed as amount determined using a standard curve.

2.5. Animal experiments

Male Sprague–Dawley rats (SLC) weighing 250–300 g were used in this study. All animals were handled in accordance with the Association for Research in Vision and Ophthalmology Statement for the Use of Animals in Ophthalmic and Vision Research after receiving approval from the Institutional Animal Care and Use Committee of the Tohoku University Environmental & Safety Committee (No. 2013MdA-218).

2.6. Implantation

The rats were anesthetized with ketamine hydrochloride (90 mg kg^{-1}) and xylazine hydrochloride (10 mg kg^{-1}). Their ocular surfaces were anesthetized with a topical instillation of 0.4% oxybuprocaine hydrochloride. A paralimbal conjunctival incision was made 1 mm from the temporal limbus. The devices were placed onto the left eyes at the sclerae. The right eyes served as controls.

2.7. In vivo release study

After implantation, the eyes were enucleated and the conjunctiva, muscle, optic nerve and the device were carefully removed. Fluorescent images were captured using a hand-held retinal camera for fluorescein angiography (Genesis-D, Kowa) to document the fluorescence distributions around the implantation site. After taking the image, the eyes were carefully separated into the retina, vitreous, lens, cornea and sclera/choroid/retinal pigment epithelium (RPE). The retina and sclera/choroid/RPE were homogenized in 100 μl of lysis buffer (1% Triton X-100 in PBS). The homogenates were centrifuged at 15,000*g* for 10 min, and the fluorescence intensity of the 80 μl of supernatant was measured spectrofluorometrically (FluoroscanAscent) ($n = 6$). For histological examination, the eyes were frozen in liquid nitrogen. A suture was placed as a landmark at the implant site of the device. After mounting the cryostat sections in a medium (Vectashield, Vector Lab), the distribution of fluorescein was observed by fluorescent microscopy (DMI6000B, Leica).

2.8. Statistical analysis

Experimental data are presented as means ± standard deviations (SD). Statistical significance was calculated with Ekuseru-Toukei 2012 (Social Survey Research Information), using the unpaired *t*-test for normally distributed isolated pairs, and the analysis of variance (ANOVA) with Tukey's test for multiple comparisons. Differences were considered significant if $p < 0.05$ (*).

3. Results

3.1. Device fabrication

The device consists of a separately fabricated TEGDM reservoir, fluorescent formulations and a PEGDM/TEGDM cover (Fig. 1c). The device was designed to deliver various formulations and dosages. In this study, sustained-release fluorescent formulations, including a single FL pellet or multiple FL/Rho/DAPI pellets (Fig. 1d), were encapsulated in the reservoir using a cover to prolong fluorescent release by limiting the rate of fluorescent dissolution within the reservoir. After loading the fluorescent pellets, the PEGDM/TEGDM prepolymer was cast over the reservoir and UV-cured to provide a seal (Fig. 1e). Because photopolymerized TEGDM is impermeable to small molecules (see below), the reservoir is a barrier that forces unidirectional fluorescent release to the sclera side.

3.2. Diffusion mechanism through the PEGDM/TEGDM system

Fig. 2a shows that the release of FL was dependent on the PEGDM/TEGDM ratio. Pure PEGDM (P100) shows the highest permeability, whereas pure TEGDM (P0) was impermeable. The release rate estimated from the slope of the curve at the initial linear state was 1296 (P100), 684 (P80), 333 (P60), 83 (P40), 35 (P20) and 0 (P0) ng day^{-1}. The release rate gradually decreased as the cumulative release approached the plateau level (10 μg ml^{-1}, maximum concentration when FL was fully released in PBS), as was seen in P100 and P80. Fig. 2b shows that the swelling ratio increased with increasing the PEGDM ratio. Fig. 2c shows the correlation of the swelling ratio, obtained from the results in Fig. 2b, with the slope obtained from the release profile results in Fig. 2a. The correlation coefficient was 0.9904, indicating almost linear correlation between the swelling ratio and release rate.

3.3. Single FL release study

Fig. 3a shows the single release profiles of FL-loaded devices that were sealed with different types of covers. Although FL-pellets without reservoir or cover showed a rapid burst-like release over 5 days, the covered devices showed a zero-order release without an initial burst. The release rate decreased with decreasing PEGDM ratio in the cover. The release rate estimated from the gradient curve for pellet, P100-, P60- and P40-covered devices were 20.7, 1.13, 0.53 and 0.10 μg day^{-1}, respectively. The results demonstrate the ability to control the release rate from a device by changing the ratio of PEGDM/TEGDM in the cover.

Devices containing FL pellet (F60) and sealed with P100, P60 and P40 covers, and pellets without reservoir or cover, were implanted onto the sclerae of rats. The devices remained at the implantation site during the experiments and were easily removed from the implantation site at the end of experiments. Routine ophthalmological examinations showed no device-related toxic effects. To demonstrate the controllability of the in vivo release of FL, images of fluorescence in the sclera after removing the device were captured by a hand-held camera (Fig. 3b). White areas corresponding to fluorescence indicate the distribution of released FL. For the pellet only, little fluorescence was observed at 1 week after implantation, probably due to the burst-like release within 5 days. For the P100-cover devices, the intensity was high at 1 week, then decreased gradually during the subsequent 3 weeks. For the P60-cover devices, the intensity was moderate for 2 weeks, then weak intensity was sustained during the remaining 2 weeks. For the P40-cover devices, weak fluorescence was sustained during 4 weeks. Trends in the fluorescence intensity were almost comparable to the in vitro release results (Fig. 3a).

Fig. 4a–d shows sectional images of an eye around the implantation site. FL (green areas) penetrated the sclera at least 1 day after implantation (Fig. 4a and c), and then reached the choroid/RPE at least 3 days after implantation (Fig. 4b and d). Intense fluorescent can be seen at the RPE, one of the blood–retinal barriers (Fig. 4d). Blurred fluorescent that passed through the RPE can be seen at the retina, indicating the passing of the molecules through the RPE into the neural retina. The amount of FL in the

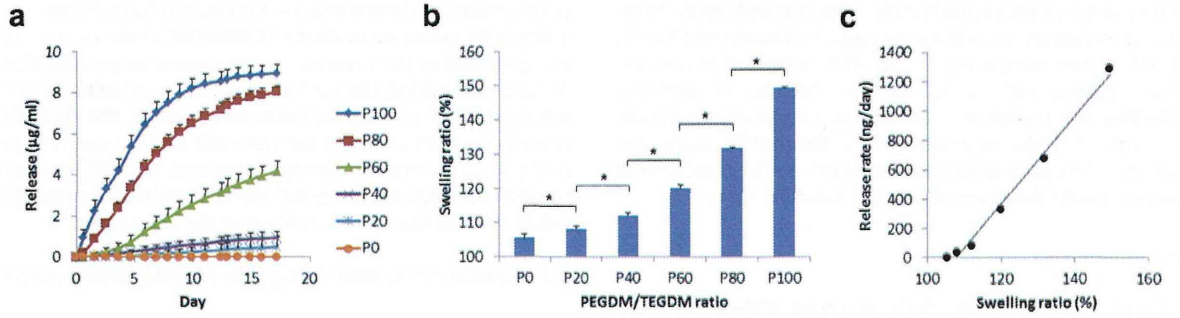

Fig. 2. (a) Permeability of FL in PBS through the PEGDM/TEGDM reservoir with various PEGDM/TEGDM ratios. The release was assessed by monitoring the increase in fluorescence in the external PBS solution with time. (b) Swelling ability in PBS of PEGDM/TEGDM polymers (size: 5 mm × 5 mm × 2 mm) with various PEGDM/TEGDM ratios. (c) Correlation between swelling ratio in (b) and release rate. Release rate was estimated from the slope of the curve of the line at the initial stable release period in (a). Values are mean ± SD. $^{*}p < 0.05$ (one-way analysis of variance (ANOVA) with Tukey's test).

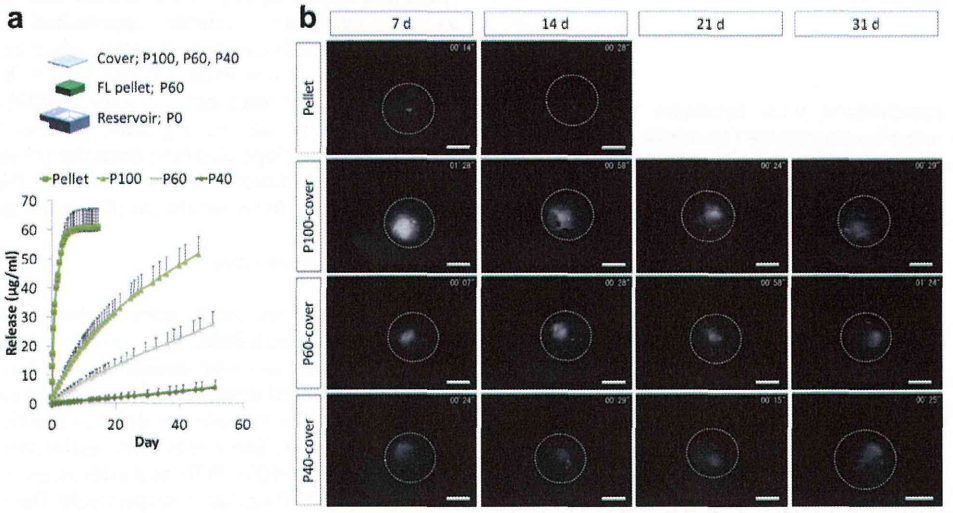

Fig. 3. (a) Release profiles of a single-drug delivery device that consists of a FL formulation pelletized with P60 and various types of cover (P100, P60 and P40), and FL pellet with no reservoir or cover. FL release was monitored spectrofluorometrically. (b) Fluorescent images of the sclera after removing the devices. Devices were implanted on the sclerae in rats for 7, 14, 21 and 31 days. White areas show released FL and circular dotted lines show the shape of the eyeball. Values are mean ± SD. Scale bars: 2 mm.

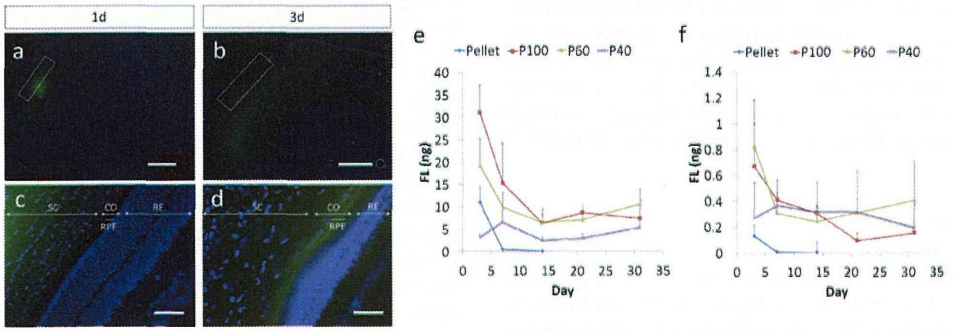

Fig. 4. The distribution of FL (green) in the retina and sclera around the implantation site (a, c) 1 day and (b, d) 3 days after implantation (square dots: device implantation site). Cell nuclei were stained with DAPI (blue). FL accumulated at RPE by day 3 after implantation and a portion of FL penetrated through the RPE and reached the retina. The amounts of FL in the sclera/choroid/RPE (e) and retinal fractions (f) during 1 month implantation. Abbreviations: sclera (SC), retinal pigment epithelium (RPE), choroid (CO) and retina (RE). Scale bars: 1 mm (a, b), 100 μm (c, d). Values are mean ± SD.

sclera/choroid/RPE, and retinal fractions during 4 weeks' implantation was measured. For the sclera/choroid/RPE fraction (Fig. 4e), the amount of FL correlated with the release profiles of the covered devices at the first week (P100 > P60 > P40). Pellet only showed almost no fluorescence after 1 week due to the burst-like release within 5 days, as is seen in Fig. 3a. From 2 weeks' implantation onwards, the amounts of FL for the P100- and P60-covered devices were at almost the same level, whereas the amount for the P40-covered device was consistently at a lower level during the successive incubation. These results are well matched with the fluorescent images on the sclera shown in Fig. 3b. For the retinal fraction (Fig. 4f), the amount of FL differed among the devices

for the first week, but was then maintained at almost the same level for each device during the following 2 weeks. Pellet only was unable to deliver FL to the retina except during the early days. After 3 weeks, the FL level for the P100-covered device was lower, while the level for the P40-covered device had decreased after 4 weeks. Although the amount of FL in the retina shows little correlation with the release profiles, the results demonstrate that fluorescent molecules released from the devices could reach the retina during the 4 weeks of implantation and the amount of FL was reduced to between 1/30 and 1/40 at the retina after passing through the sclera.

3.4. Multiple FL/Rho/DAPI release study

The simultaneous independently controlled multiple release was tested using three kinds of fluorescents, FL, Rho, and DAPI, which may mimic low-molecular-weight drugs. The device was filled with three kinds of pellets, each with different ratios of PEGDM/TEGDM. The release profiles of each pellet are shown in Supplementary Fig. S.2. DAPI pelletized with P100 (D100) was always included in the device as a constant control. FL was pelletized with P100 (F100), P70 (F70) and P60 (F60). Rho was also pelletized with P100 (R100), P70 (R70) and P60 (R60). Fig. 5a–c shows that the release rate of the molecules can be tuned by changing the composition of each pellet. For example, the release rate of FL or Rho varied as the PEGDM ratio changed (Fig. 5a vs. Fig. 5b), whereas that of DAPI was constant. When the device was sealed with a P60 cover, the absolute amount released decreased to between one-fourth and one-eighth in all of the devices compared to the P100-covered devices, but importantly, the ability to independently control the release rates of the molecules was maintained (Fig. 5d–f). If the release results were sorted for each molecule, the release kinetics of each molecule was always dependent on the PEGDM/TEGDM ratio of the pellet (Supplementary Fig. S.3). These results indicate that the release kinetics can be tuned via two independent diffusion mechanisms afforded by a sustained-release formulation and a controlled release cover.

Devices containing a combination of F60/R40/D60 pellets (device A) or F60/R60/D40 pellets (device B), sealed with a P60 cover, were implanted onto the rat sclerae. Fig. 6a–h shows the sectional images for 1 and 4 weeks after implantation. Magnified images showed fluorescence at the outer nuclear layer (ONL) in the retina and the intensity of the fluorescence correlates with device condition; device A, which releases DAPI at a faster rate than device B, shows more intense blue fluorescence in the ONL compared with device B (Fig. 6b and f). On the other hand, device B, which releases Rho at a faster rate than device A, exhibits more red fluorescence in the retina than that of device A (Fig. 6d and h). Low magnification images of the sections showed the local distribution of released fluorescents around the implantation site 1 and even 4 weeks after implantation (Fig. 6a, c, e and g). This may indicate that the released drug is specifically delivered to the retina local to the implantation site.

The amounts of fluorescence in the sclera/choroid/RPE (Fig. 7a–c) and the retina fractions (Fig. 7d–f) at 1, 2 and 4 weeks after implantation were measured. Because FL was set to release at the same rate in each device, there was no significant difference between the amount of FL detected in the fractions for device A or B (Fig. 7a and d). On the other hand, the amount of Rho in sclera/choroid/RPE and retinal fractions for device B was higher than for device A, and at 4 weeks' implantation a significant difference (p value: 0.042) can be seen in the sclera/choroid/RPE fraction (Fig. 7b). Similarly, the amount of DAPI for device A was significantly higher than for device B at 4 weeks' implantation (p value; 0.037) (Fig. 7c). There was no difference between Rho and DAPI intensities in the retina for the devices (Fig. 7e and f).

4. Discussion

We established a transscleral multi-drug delivery device with which we demonstrated the transport of low-molecular-weight compounds into the ocular tissue using fluorescents. The release of multiple drugs can be tuned by changing the formulations of the drug as well as the covering. The ability to control the release of fluorescents from the PEGDM/TEGDM system may be explained by the results of swelling tests (Fig. 2). The polymers made of short chains of TEGDM are likely to be compact, with little ability to swell, and impermeable to low-molecular-weight compounds. On the other hand, long chains of PEGDM may result in more open polymer networks, showing a greater tendency to swell, facilitating permeation of small molecules. Further, the release rate of each fluorescent differs, even when we used the same pelletized

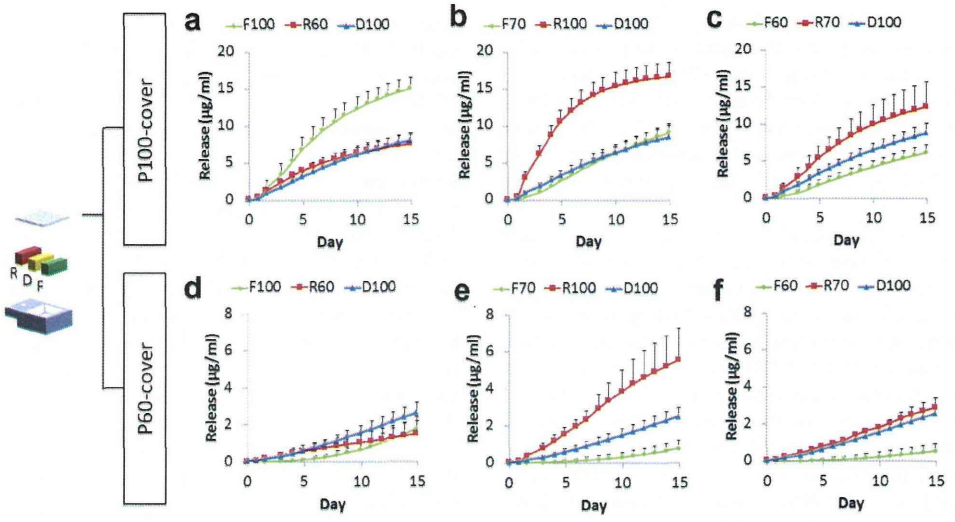

Fig. 5. (a–f) Release profiles of a multi-drug delivery device that consists of three types of fluorescent pellets (FL, Rho and DAPI, designated F, R and D, respectively, in the schematic) made of various PEGDM/TEGDM content, and two types of cover (P100 cover: (a–c), P60 cover: (d–f)). DAPI was pelletized with P100 as a constant release control. FL and Rho were pelletized with P100, P70 and P60, respectively. Values are mean ± SD.